



Training-free referenceless camera image blur assessment via hypercomplex singular value decomposition

Lijuan Tang^{1,2} · Qiaohong Li³ · Leida Li¹ · Ke Gu³ ·
Jiansheng Qian¹

Received: 14 August 2016 / Revised: 14 December 2016 / Accepted: 3 February 2017 /

Published online: 16 February 2017

© Springer Science+Business Media New York 2017

Abstract Blur plays an important role in the perception of camera image quality. Generally, blur leads to attenuation of high frequency information and accordingly changes the image energy. Quaternion describes the color information as a whole. Recent researches in quaternion singular value decomposition show that the singular values and singular vectors of the quaternion can capture the distortion of color images, and thus we reasonably suppose that singular values can be utilized to evaluate the sharpness of camera images. Motivated by this, a novel training-free blind quality assessment method considering the integral color information and singular values of the distorted image is proposed to evaluate the sharpness of camera images. The blurred camera image is first converted to LAB color space and divided into blocks. Then pure quaternion is utilized to represent pixels of the blurred camera image and the energy of every block are obtained. Inspired by the human visual system appears to assess image sharpness based on the sharpest region of the image, the

✉ Jiansheng Qian
qianzhangqiqa@163.com

Lijuan Tang
ntlj@163.com

Qiaohong Li
QLI013@e.ntu.edu.sg

Leida Li
lileida@cumt.edu.cn

Ke Gu
gukesjtuee@gmail.com

¹ School of Information and Control Engineering, China University of Mining and Technology, Xuzhou, 221116, China

² School of Electrical and Information, Jiangsu Vocational College of Business, Nantong, 226011, China

³ School of Computer Science and Engineering, Nanyang Technological University, Singapore, Singapore

local sharpness normalized energy is defined as the sharpness score of the blurred camera image. Experimental results have demonstrated the effectiveness of the proposed metric compared with popular sharpness image quality metrics.

Keywords Hypercomplex · Singular value decomposition (SVD) · No-reference (NR) · Image quality assessment (IQA) · Energy

1 Introduction

The rapid development of Internet business and multimedia technology makes images play an important role in human daily life. However, images are often degraded by different kinds and levels of distortion in the procedure of acquisition, transmission, compression, reconstruction and storage. Hence, it is urgent to develop effective and efficiency image quality assessment(IQA) metric to assess image quality so that it can be used for many image processing applications, such as image compression [31], search [47], forensics [17, 51].

In the past decades, scientists have proposed many image quality metrics which can be basically classified into subjective and objective quality assessment methods. Subjective quality assessment is creditable for human beings are the final consumers, but it is expensive and difficult to implement in-service applications. Therefore, objective IQA model has attracted more attention in recent years. Depending on the validity of reference images, objective IQA metrics can be further divided into full reference (FR), reduced-reference (RR) and no reference/blind (NR) quality assessment methods [15]. FR IQA methods utilize the distortion-free image to assess the distorted image, which works on the assumption that the reference image exists [1].

But in most cases, such as video on demand business or broadcast service on the Internet, only the deteriorated image can be acquired, this kind of IQA models belongs to NR/blind IQA methods. Furthermore, according to the prior distortion types of the image, blind IQA models can be further divided into distortion-specific and general purpose methods. Typical distortion-specific NR IQA methods are devoted to blurriness/sharpness [2, 8, 19, 35, 41], blockiness [21], ringing effect [22], contrast distortion [7, 12], etc. Recently, general-purpose blind methods have been an popular research field. Many blind IQA methods have been proposed in [4, 10, 11, 18, 24–26, 34, 42, 50].

Different from the aforementioned methods, RR IQA methods use partial of the reference image to assess the deteriorated image which resorts to a good tradeoff between effective and efficiency. Many RR IQA models have also been proposed in [12, 40]. Yet in most real-world scenarios, the original image (full or partial) is not available. By contrast, NR methods can assess distorted image quality without original image, so they are highly desired in reality applications. This paper focuses on NR camera sharpness assessment.

Sharpness is a key factor in the process of evaluating the quality of camera images [42]. Although the causes of blur are variety (e.g. target simple motion or complex motion, image compression and camera out-of-focus), blur is typically characterized by the propagation of the edge width and consequently caused the high frequency information attenuation. Mariziliano et al. [23] proposed a sharpness method based on the analysis of the sharp edges and adjacent regions in an image. The Sobel operator was used to find strong edges and their positions, then the local blur values over all edges found was used to obtain the sharpness score. Vu et al. [45] devised a fast image sharpness (FISH) metric by using wavelet

transformation to evaluate the blur level of distorted image. The input distorted image was first decomposed via the discrete wavelet transform (DWT), then the energies of the DWT subbands was computed. Finally, a weighted function for the three-level log-energies was utilized to obtain the final sharpness score. The concept of Just Noticeable Blur (JNB) was introduced by Ferzli et al. [5]. The JNB metric combined a probability summation model with the just noticeable blur to evaluate the amount of blurriness in distorted images. An extension of JNBM was the cumulative probability of blur detection (CPBD) metric which through pooling the localized probability of blur [27]. Hassen et al. [14] addressed a sharpness metric by utilizing Local Phase Coherence. For the blur destroyed the LPC structure of an image, the sharpness can be computed by the strength of LPC.

A sharpness metric named the singular value curve (SVC) was proposed by Sang et al. [36]. Since blur can affect the singular values significantly, and the SVC can be utilized to evaluate the degree of blur. The spectral and spatial sharpness (S3) metric was addressed by Vu et al. [46]. The attenuation degree of high-frequency information was measured by the slope of magnitude spectrum, and contrast was measured by the total spatial variation. Then a weighted geometric mean was used to integrate the total spatial variation and the slope of the magnitude spectrum for image sharpness assessment. Li et al. [19] provided a blind image sharpness method based on discrete orthogonal moments. The gradient of a blurred image is first computed, then the Tchebichef moments are computed to describe image shape. Finally, the variance-normalized moment energy is defined as the image blur score. A NR sharpness method in the autoregressive parameter space was proposed by Gu et al. [8]. It first calculated the energy and contrast differences in the locally estimated AR coefficients in a point-wise way, then the image sharpness score is acquired by percentile pooling.

Although existing image blur metrics are good in simulated blur distortion, they poorly perform for realistic camera image assessment, which can be found from experimental results in Section 4. Realistic camera images contain not only typical distortions which is easy to modeled, but also more complicated and realistic ones. Sample realistic camera images chosen from the BID database [3] are illustrated in Fig. 1.

It can be observed from the Fig. 1 that realistic camera blur distorted images contain many categories of blur distortions. Image (a) may be classified into the simple motion class that could be fairly considered linear caused by camera movements. Image (b) consists of complex motion blur which caused by complex motion paths. Image (c) belongs to out of focus category which caused by the whole image is out of focus. Image (d) contains complex blur distortion which may contains any other types of degradation. Hence, it is challenging to evaluate realistic camera blur images.

In this work we focus on blind realistic camera images sharpness evaluation. Compared with previous works, this paper is the first work to propose a blind sharpness of camera images based on quaternion singular values decomposition which considers the inevitable influence of color information on the sharpness evaluation. Furthermore, the proposed blind quaternion singular value decomposition metric (BQSVD) can acquire sharpness scores highly consistent with the human visual system (HVS).

The remainder of this paper is arranged as follows. In Section 2, the theories of the related algorithms employed in this paper is presented. The description of the proposed metric is introduced in Section 3. In Section 4, thorough experiments are conducted on the BID database to verify the performance of our BQSVD model with recently devised blind sharpness IQA methods. Future works and conclusions are given in Section 5.

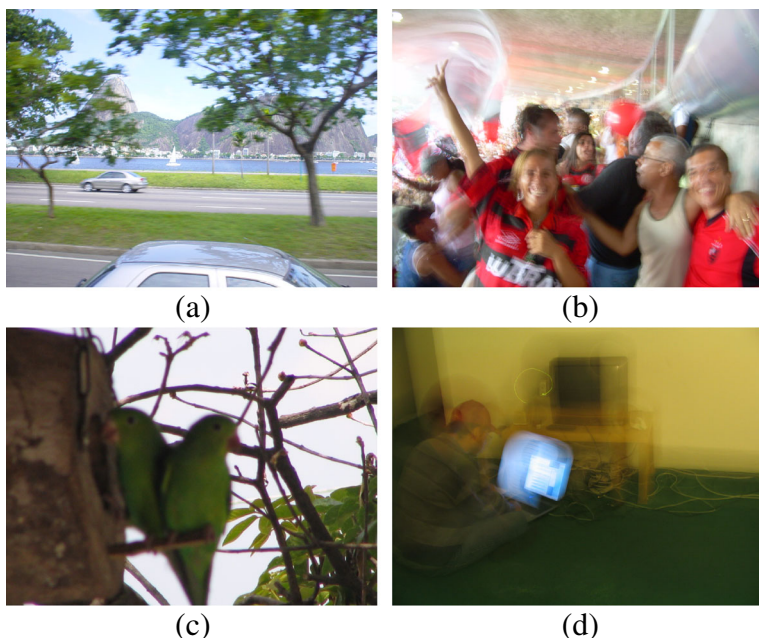


Fig. 1 Sample realistic blur images from the BID database [3]. **a** Simple motion blur. **b** Out of focus blur. **c** Complex motion blur. **d** Other complicated distortions

2 Quaternion singular value decomposition

2.1 Feature extraction by singular value decomposition

Objective quality assessment method generally consists of two steps, including feature extraction and feature pooling to obtain a scalar index as image quality score. First step, features extraction plays a critical role for objective perceptual quality assessment which should effectively reflect the changes of image quality. The second step decides the relationship between the features and the image quality. Various transforms can be utilized to extract features, such as singular value decomposition (SVD) [39], discrete wavelet transform (DWT) [26], discrete cosine transform (DCT) [34], discrete Fourier transform (DFT) [29], etc. Basically speaking, the changes in transformation coefficients can be utilized to measure visual quality. For DCT and DFT transforms, base images are same for all the images in the frequency domain. However uses the unique base images for each image. Hence, SVD is more advantageous for description visual signal and has been successfully applied to statistics and signal processing field [30].

SVD is a kind of famous transformation in linear algebra. Formally, the mathematical definition of SVD for an image matrix $W_{m \times n}$ can be defined as

$$W_{m \times n} = U_{m \times m} S_{m \times n} V_{n \times n} \quad (1)$$

where U and V are unitary matrix, S is a diagonal matrix, the diagonal entries σ_i are listed in descending order and known as the singular values of W . We can define U and V to be

$$\begin{aligned} U &= [u_1, \quad u_2, \quad \cdots \quad u_m] \\ V &= [v_1, \quad v_2, \quad \cdots \quad v_n]. \end{aligned} \quad (2)$$

The columns of U and V are orthonormal bases. The matrix UV^T can represent the image structure (the base image), while the singular values σ_i are the weights assigned to these base images [28]. To visually view the effect of singular value and singular vector on the image, we show examples in Figs. 2 and 3. Figure 2 shows the singular values σ_i are mainly reflect the luminance variations in images, which can also reflect variations in the frequency components of the image. We can observe from Fig. 3 that the first few singular vectors determines the image main structure, while following decide the image details [28].

Since singular vectors and singular values can describe features of images, which may be used for quality assessment. In the literature, several SVD-based image quality methods have been proposed. Shnayderman et al. [39] proposed an SVD-based gray IQA metric mainly focus on computing the distance between the singular values of the distorted image block and the original image block. In [43], the authors used the singular value decomposition algorithm to calculate the ratio of the first and second largest eigenvalues to measure image distortion. Qureshi et al. [33] proposed a blind blur assessment method based on higher order singular values. A third-order tensor was utilized to exploit the spatial and

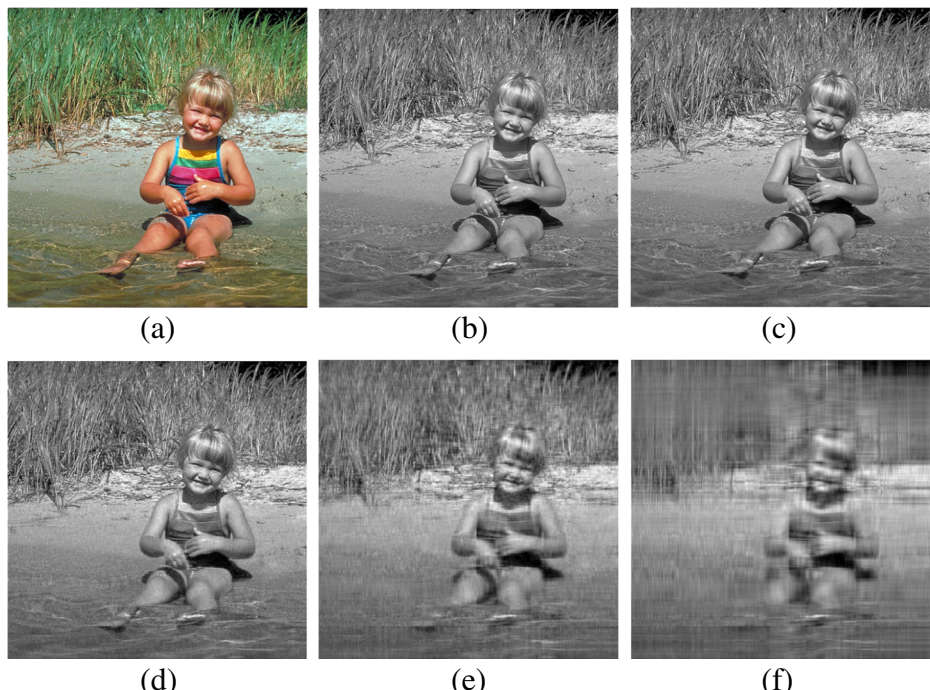


Fig. 2 Effect of changing singular values σ . The original image is shown in (a). The number of σ_i set as (b) $i = 512$. (c) $i = 200$. (d) $i = 100$. (e) $i = 30$. (f) $i = 10$

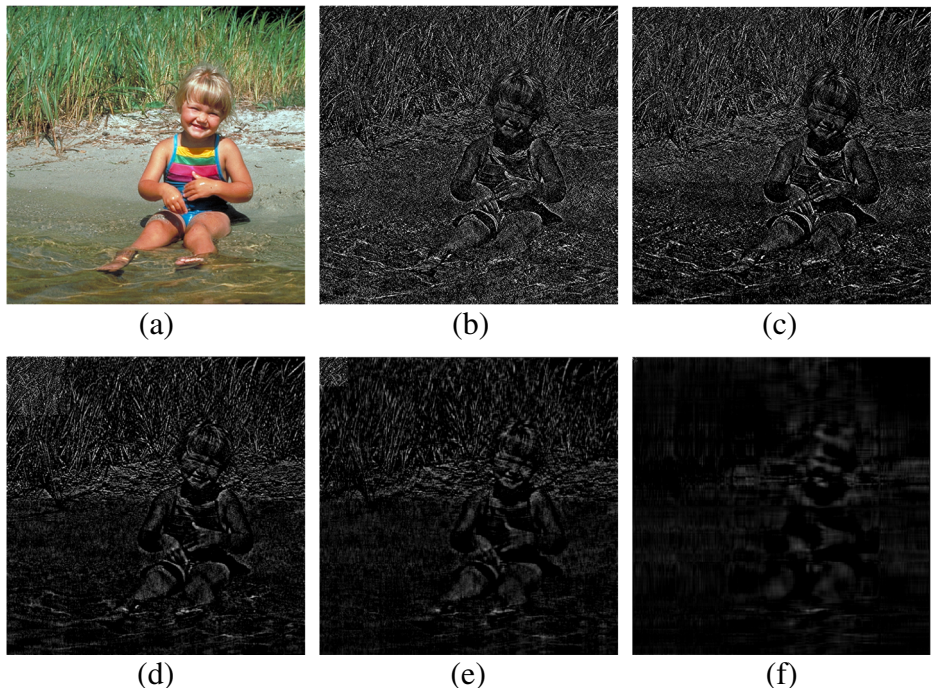


Fig. 3 Effect of changing $\mathbf{U}\mathbf{V}^T$ values. **a** Child-swimming image. The number of group $U_i V_i^T$ set as **(b)** $i = 512$. **c** $i = 300$. **d** $i = 100$. **e** $i = 50$. **f** $i = 10$

inter-channel correlations of an RGB color image for evaluating the quality of the distorted image. Recently, Wang et al. [48] proposed an image quality metric based on the standard deviation of singular values for it can effective reflect image structure change.

2.2 Quaternion model

The concept of quaternion was proposed by Hamilton in 1843 [13]. Quaternion is an expansion of complex, namely hyper complex. A quaternion is consisted of two parts, the real part and the imaginary part which can be described by

$$Q = x + yi + zj + wk \quad (3)$$

where i , j and k are the imaginary units, x , y , z and w are real numbers. Due to the relations between the three imaginary parts, the multiplication of quaternions does not satisfy the commutative law. The multiplication rules between the three imaginary numbers are:

$$\begin{aligned} ki &= -ik = j \\ jk &= -kj = i \\ ij &= -ji = k \\ i^2 &= j^2 = k^2 = ijk = -1 \end{aligned} \quad (4)$$

There are other notations for quaternions [13]. Another representation of a quaternion Q can be defined as

$$Q = \alpha + \beta j \quad (5)$$

where $\alpha = x + yi \in C$ and $\beta = z + wi \in C$. This is known as Cayley-Dickson notation for quaternion matrix. The conjugate of a quaternion is defined as

$$\overline{Q} = x - yi - zj - wk. \quad (6)$$

A pure quaternion is the case with a null real part (the first real number $x = 0$). Pure quaternion is widely used to represent color image, which the three channels of the color image (red, green and blue) [37] are represented by the three imaginary parts. So the pure quaternion represents a color image I as following:

$$Q_I = F_R i + F_G j + F_B k \quad (7)$$

where R , G and B denotes the three channel of red, green and blue, respectively.

2.3 Quaternion singular value decomposition

SVD is used to decompose a matrix. Hence, it can be directly applied on gray images. For a color image, one way is to directly operate SVD on one channel of the color image, and another way is through transforming the color image to extract the brightness level information before using the SVD method to deal with. Both of the two ways cannot handle the color image as a whole, neglecting the color information of the color image. However, the quaternion model can describe the color image information as a whole, according to the definition of SVD on the complex adjoint matrix, quaternion singular value decomposition (QSVD) can be utilized to assess color images quality [32]. QSVD of a quaternion Q is defined as follows [37]:

$$F_{Q(m,n)} = U_{m \times m} S_{m \times n} \begin{pmatrix} \sum_r & 0 \\ 0 & 0 \end{pmatrix} V_{n \times n}^* \quad (8)$$

$$\begin{aligned} U &= [u_1, \quad u_2, \quad \cdots \quad u_m] \\ V &= [v_1, \quad v_2, \quad \cdots \quad v_n], \end{aligned} \quad (9)$$

$$\sum_r = diag(\sigma_1, \sigma_2, \cdots, \sigma_r) \quad (10)$$

where \sum_r is a diagonal matrix, the diagonal entries σ_i are the singular values of the quaternion matrix $Q(m, n)$ and r is the rank of $Q(m, n)$. V and U are the right and left singular vectors of quaternion matrix $Q(m, n)$ and elements of these two unitary matrixes are all quaternions. $*$ denotes the conjugate transpose.

To intuitional understanding the gray scale SVD which only concentrated on luminance information, and QSVD combined luminance and chrominance information into the IQA model, we give an example in Fig. 4. The subsequent formula is used to construct the distortion map [39].

$$D(i) = \sqrt{\sum_{i=1}^P (S_{dis}(i) - S_{org}(i))^2} \quad (11)$$

where S_{org} denotes the original image blocks' singular values, S_{dis} denotes the singular values which are obtained by gray scale SVD and QSVD method of the distorted block, P is the size of block . The set of distances D_i , when displayed in graph by mapping D_i values to the range $[0, 255]$, a gray scale image can be obtained which represents distortion map.

It can be observed from the figure that the gray scale SVD method which only extracts the luminance components and discards many effective components, even can not intuitional represent the distortion level. However, QSVD performs better, which implies that the chrominance information should be considered when assess color image quality.

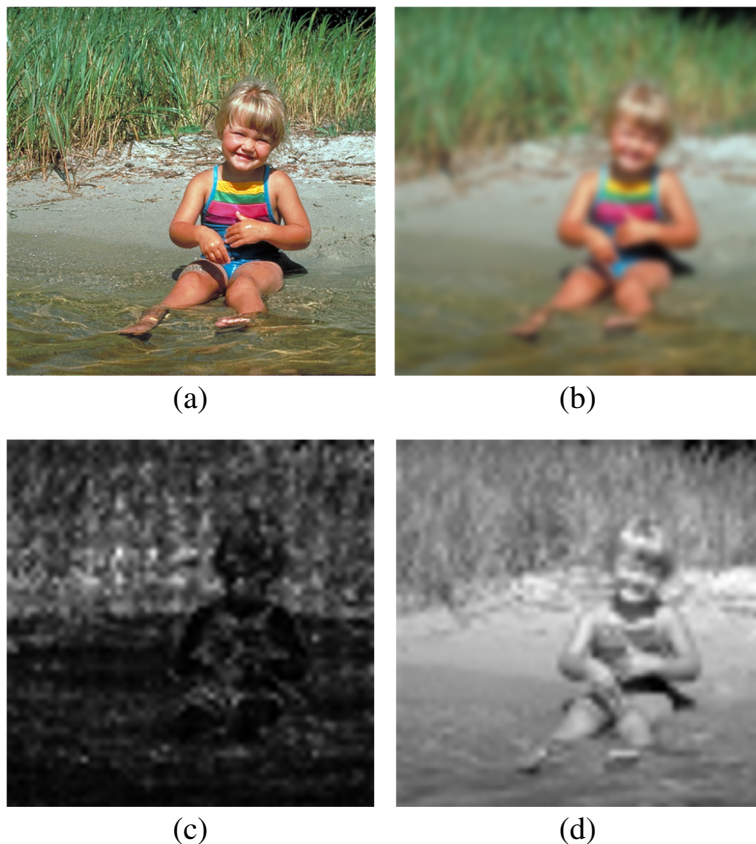


Fig. 4 **a** and **(b)** are the child-swimming image and the corresponding blur distortion image. **c** and **(d)** are the distortion maps of the gray scale SVD and QSVD of the blur distorted images, respectively

3 The proposed blind quality metric

So far, many IQA metrics have been proposed for objective IQA. They are good in simulated distortions, but poorly perform for realistic camera image assessment. Camera images have complex distortion, like the effect of color crosstalk which causes blur with desaturation is difficult to measure [16]. In this paper QSVD is employed to evaluate the sharpness of realistic camera images. The theoretical foundation is that Frobenius norm of hyper complex matrix can be used to represent the energy of color camera images, and we have a reason to believe energy change can be effectively reflect the extent of blur.

3.1 Color space transformation

In our work, a novel hyper complex SVD-based blind camera image assessment metric is proposed. Figure 5 shows the flowchart of the proposed metric. It includes three main stages. First, the input blurred image is converted into LAB color space, and is represented by pure quaternion. Second, two components are calculated: 1) quaternion singular values for

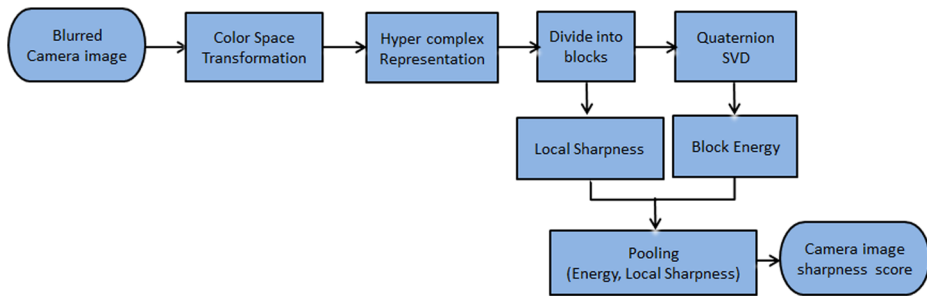


Fig. 5 Flowchart of the proposed camera image sharpness metric

blocks; 2) variances of the realistic blur camera image for blocks. Finally, effective pooling method is utilized to acquire the blur score of the input blurred camera images.

According to the previous researches, scientists found that the HVS is much more sensitive to the change of luminance than the change of chrominance [39]. Therefore, most previous IQA methods were devised based on the mathematical modeling. Our metric considers the inevitable influence of color information on the sharpness assessment. So, in the proposed metric, the blurred camera image is first converted into widely used LAB color space [38].

Since the LAB color space is designed to approximate human vision system, unlike the RGB and CMYK color space, it includes all the colors visible to the naked eye and creates a model that is independent of the device [9]. The LAB model is a three-dimensional model, and L, A and B nonlinear relationship is used to simulate the nonlinear response of the eye. The three coordinates of LAB represents the color brightness, the transition between red and green, and the transition between yellow and blue. There is no simple formula for conversion between RGB and LAB, because the RGB model is dependent on the device. Therefore, the RGB values must first be converted to the data which is independent of the device, then it can be converted to the LAB color space.

The transformation can be defined as follows [38]:

$$\begin{aligned} B &= 200[f(Y/Y_n) - f(Z/Z_n)] \\ A &= 500[f(X/X_n) - f(Y/Y_n)] \\ L &= 116f(Y/Y_n) - 16 \end{aligned} \quad (12)$$

where

$$f(t) = \begin{cases} t^{1/3} & \text{if } t > (\frac{6}{29})^3 \\ \frac{1}{3}(\frac{29}{6})^2t + \frac{4}{29} & \text{otherwise} \end{cases} \quad (13)$$

where X_n , Y_n and Z_n are the $CIEXYZ$ tristimulus values of the reference white point. Under Illuminant D65, the values are $X_n = 95.047$, $Y_n = 100.000$, $Z_n = 108.883$.

The domain of the function $f(t)$ is divided into two parts which is to prevent an infinite slope at $t = 0$. $f(t)$ was supposed to match both value and slope of the $t^{1/3}$ part of the function at t_0 . In other words:

$$t_0^{1/3} = at_0 + b, \quad (14)$$

$$\frac{1}{3}t_0^{-2/3} = a. \quad (15)$$

Equation (14) matches in value and (15) matches in slope. The above two equations can be solved for a and t_0 :

$$a = \frac{1}{3}\delta^{-2} = 7.787037\dots \quad (16)$$

$$t_0 = \delta^3 = 0.008856\dots \quad (17)$$

where $\delta = 6/29$ [38].

3.2 Quaternion representation and image energy

After the transformation, the pure quaternion is used to express every pixels of the transformed blurred camera image:

$$F_Q = F_L i + F_A j + F_B k \quad (18)$$

where L , A and B are the three channels of LAB. It is well known that Frobenius norm can be utilized to represent the energy E of a matrix F_Q :

$$E = \|F_Q\|_F. \quad (19)$$

Therefore, Frobenius norm of hyper complex matric F_Q can be used to represent the energy of color camera images. Following the definition of the hyper complex SVD, for any hyper complex matrix $F_Q \in H^{M \times N}$, there exists two unitary hyper complex matrix U and V ,

$$F_Q = U \begin{pmatrix} \sum_r & 0 \\ 0 & 0 \end{pmatrix} V^* \quad (20)$$

where $U \in H^{M \times M}$, $V \in H^{N \times N}$. Superscript $*$ denotes conjugate transpose, \sum_r is a diagonal matrix that contains the number of r non-empty values. According to (19) and (20), the energy of color camera image can be defined as:

$$\begin{aligned} E &= \|F_Q\|_F \\ &= \|U \cdot \begin{pmatrix} \sum_r & 0 \\ 0 & 0 \end{pmatrix} \cdot V^*\|_F \\ &= \|U\|_F \cdot \left(\begin{pmatrix} \sum_r & 0 \\ 0 & 0 \end{pmatrix} \right) \|_F \cdot \|V^*\|_F \\ &= \left\| \begin{pmatrix} \sum_r & 0 \\ 0 & 0 \end{pmatrix} \right\|_F. \end{aligned} \quad (21)$$

Since U , V is unitary hyper complex matrix, their Frobenius norm equals to 1. According to (21), the energy of color camera image can be decided by the Frobenius norm of hyper complex matrix singular values. In other words, the singular values of hyper complex matrix denotes the energy feature of the color image, and it can be utilized as benchmark for assessing color image quality. It serves as the theoretical basis for our proposed blind camera sharpness assessment metric.

Blur leads to the decrease of high frequency information of the image, and the quaternion singular values change accordingly account for the variations of energy. To illustrate the relation between quaternion singular values and blur, an example is shown in Fig. 6, in which three realistic camera images with different blur scales and their energy are shown. It is can be observed from the figure that the energy change with the degree of blur. Therefore, the energy can be utilized to test the degree of sharpness with the same scene.

To acquire a blind sharpness method, the influence of image scene or the complex of image content should be considered. Inspired by Hassen et al. research [14], humans seem

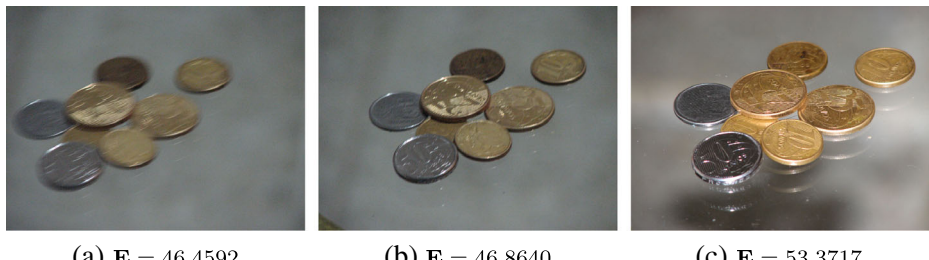


Fig. 6 Three realistic camera images and their average energies of blocks for the same content images with different extent of blur

to make judgement of image quality based on the sharpest region, the method in [25] is adopted to select a collection of blocks which contains rich information. Specifically, an image I is preprocessed by the natural scene statistical (NSS) model as follows [49]:

$$\hat{I}(m, n) = \frac{I(m, n) - \mu(m, n)}{\sigma(m, n) + 1} \quad (22)$$

where m and n are spatial indices, and

$$\mu(m, n) = \sum_{k=-K}^K \sum_{l=-L}^L \omega_{k,l} I(m+k, n+l) \quad (23)$$

$$\sigma(m, n) = \sqrt{\sum_{k=-K}^K \sum_{l=-L}^L \omega_{k,l} [I(m+k, n+l) - \mu(m, n)]^2} \quad (24)$$

are the local mean and standard deviation, where $\omega = \{\omega_{k,l} | k = -K, \dots, K, l = -L, \dots, L\}$ is a 2D Gaussian weighting function. Because $\sigma(m, n)$ contains rich image structure information, it is used to gauge the local sharpness.

In this work, we utilize the mean opinion score(MOS) as the subjective evaluation, which is obtained by averaging subjective scores given by human observers. An example shown in Fig. 7a-d, these images have similar MOS values with similar extent of blur, but their energies differ significantly. Hence, to eliminate the influence of image scene, the local image sharpness is utilized to normalize the total energy. Figure 7e shows the energy of the image (a)-(d), and the corresponding local sharpness normalized energy is shown in Fig. 7f. We can seen from the Fig. 7e that the original energy without normalization fails to predict the sharpness of image with different scenes. But after using the local sharpness (24) normalized the energies, the predicted sharpness scores are similar. Hence, it can effectively assess the blur level of images with different image scenes.

3.3 Sharpness score based image energy

In summary, the proposed BQSVD algorithm can be summarized below. For a realistic blur camera image in RGB color space, it is first converted into LAB color space. Next, the image is segmented into non overlapping blocks of the same size for the essential low order statistics of images can be captured by local image patches. The size of the block used

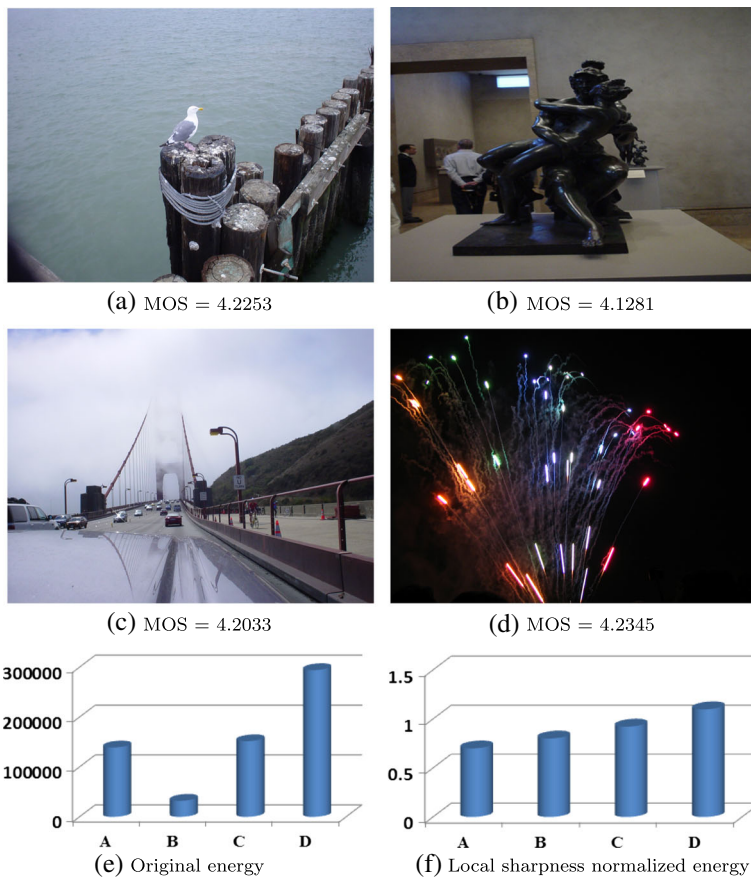


Fig. 7 Four realistic camera images with similar MOS values together with the original energy and local sharpness normalized energy

in the proposed metric is 8×8 , since the standard block size used in the JPEG compression and many image processing applications are all 8×8 based. The pure quaternion is used to represent the three channel L , A and B . The block set is denoted by C_j , where $j \in 1, 2, 3, \dots, P$, $P = 3 * \lfloor M = m/8 \rfloor \times \lfloor N = n/8 \rfloor$, m and n are the image dimensions, and $\lfloor \cdot \rfloor$ is the floor operation. Then the local sharpness of the blocks in C_j are calculated. Because the HVS generally inclines to make judgement of the whole image sharpness according to the sharpest regions [6, 45, 46], the $t\%$ highest local sharpness blocks are utilized to obtain the sharpness score as following:

$$S_{BQSVD} = \frac{\sum_{k=1}^T E_k}{\sum_{k=1}^T (\sum \sum_{(i,j) \in patchk} \sigma(i, j))} \quad (25)$$

where $T = \lfloor t\% \times P \rfloor$ denotes the number of first high local sharpness blocks, S_{BQSVD} is the sharpness score, E_k and σ denote the energy and local sharpness of the k^{th} block which can be obtained by (21) and (24), respectively.

4 Experimental results and discussions

4.1 Experimental settings and protocol

The performance of the proposed method is tested on the realistic blur database (BID) camera image quality database [3]. The images in this database are obtained for a various camera apertures, scenes, varying exposure times and lighting conditions. The BID database includes 586 images with resolutions ranging from 640×480 to 2816×2112 pixels which contains many kinds of complex and realistic blur. And mean opinion scores of the images in BID database are ranging from 0 to 5.

According to the VQEG suggestions [44], four criterions and five parameter nonlinear fitting function are utilized to test the performance of the proposed metric. The four criterions including Pearson linear correlation coefficient (PLCC), Spearman rank order correlation coefficient (SRCC), Kendall's rank correlation coefficient (KRCC), and root mean square error (RMSE).

The first Pearson's (linear) correlation coefficient (PLCC) for prediction accuracy, which is defined as

$$\text{PLCC} = \frac{\sum_i (q_i - \bar{q})(s_i - \bar{s})}{\sqrt{\sum_i (q_i - \bar{q})^2 \sum_i (s_i - \bar{s})^2}} \quad (26)$$

where s_i and \bar{s} are the i -th image's subjective rating and the mean of the overall s_i ; q_i and \bar{q} are the i -th image's converted objective score after nonlinear regression and their mean value.

The second Spearman's rank ordered correlation coefficient (SRCC) for prediction monotonicity. SRCC is calculated by

$$\text{SRCC} = 1 - \frac{6}{N(N^2 - 1)} \sum_{i=1}^N d_i^2 \quad (27)$$

where N denotes the image number in the testing database; d_i is the difference between the i -th image's ranks in objective and subjective evaluations.

The third Kendall's rank correlation coefficient (KRCC) is another criteria to measure the prediction monotonicity:

$$\text{KRCC} = \frac{F_a - F_d}{1/2F(F - 1)} \quad (28)$$

where F_a and F_d denote the number of accordant and dissonant pairs in the testing data set.

The last root mean square error (RMSE) is another criteria to measure the prediction accuracy. The RMSE is calculated by

$$\text{RMSE} = \sqrt{\frac{1}{n} \sum_i (x_i - y_i)^2} \quad (29)$$

where x_i denotes MOS values and y_i denotes the predicted score. In order to calculate these values, a monotonic logistic function is adopted to provide a mapping between objective scores and subjective scores [44].

$$f(y) = \alpha_1 \left(\frac{1}{2} - \frac{1}{1 + e^{\alpha_2(y - \alpha_3)}} \right) + \alpha_4 y + \alpha_5 \quad (30)$$

where y denotes the original objective score, $f(y)$ denotes the fitted score, and α_i ($i = 1, 2, 3, 4, 5$) are regression parameters to be fitted.

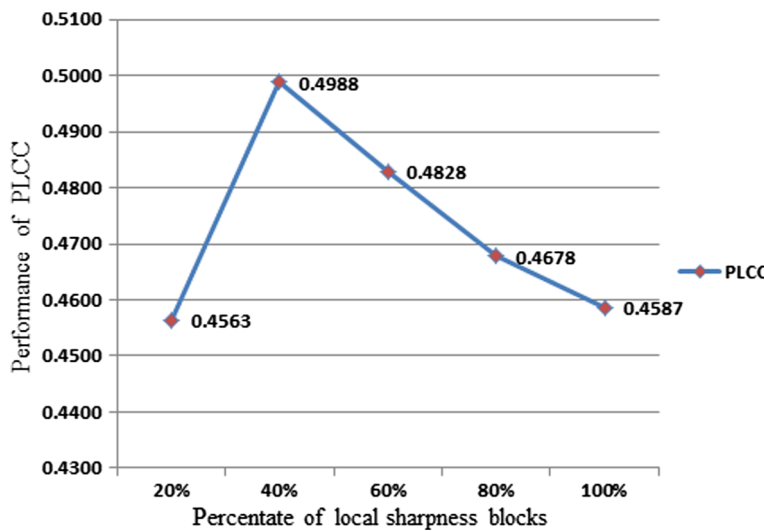


Fig. 8 The computed curves of PLCC with different percentage of high local sharpness blocks

Because the proposed metric evaluates image sharpness based on the sharpest blocks, it is necessary to decide the optimal percentage of blocks($t\% \times K$). Therefore, we conducted an experiment on BID database to observe how the metric performs with the change of the number of blocks. Generally, the selected areas should not less than one fifth of the image size for maintaining the semantic information. We also test the number of blocks from 40 % to 100 % and the simulation results are shown in Fig. 8.

Figure 8 shows that PLCC values increase with the number of blocks range from 20 % to 40 %. Then with the number of blocks increase, PLCC values decrease inversely. It illustrates that HVS tends to determine the sharpness of an image based on the sharpest areas [6, 45, 46]. Based on this finding, the proposed method employs 40 % high variance blocks in implementation and is applied in the subsequent experiments.

Table 1 Performance comparison with seven state-of-art blind sharpness metrics on the BID database

Metric	PLCC	SRCC	KRCC	RMSE
S3 [46]	0.4270	0.4253	0.2921	1.1320
LPC [14]	0.3901	0.3161	0.2161	1.1528
MLV [2]	0.3103	0.3201	0.2209	1.1901
SVC [36]	0.4295	0.3581	0.2412	1.1306
CPBD [27]	0.2704	0.2711	0.1820	1.2053
JNBM [5]	0.2608	0.2317	0.1582	1.2086
ARISM [8]	0.1841	0.1841	0.1258	1.2305
BIBLE [20]	0.3816	0.3846	0.2611	1.1572
Marziliano [23]	0.1352	0.0827	0.0535	1.2404
BQSVD (Pro.)	0.4988	0.4934	0.3379	1.0851

The best performed metric is highlighted with boldface

Table 2 The performance of the proposed method using different color space representation

Color Space	PLCC	SRCC	KRCC	RMSE
Gray Scale	0.3386	0.3066	0.2069	1.1780
RGB	0.3439	0.3072	0.2069	1.1756
YIQ	0.3308	0.3013	0.2029	1.1815
LAB	0.4988	0.4934	0.3379	1.0851

4.2 Comparison with blind sharpness IQA metrics

In this section, the proposed model is carried out on the BID database and compared with the popular blind sharpness metrics, including MLV [2], S3 [46], ARISM [8], BIBLE [20], JNBM [5], LPC [14], Marziliano [23], SVC [36] and CPBD [27].

Table 1 lists the results, and the best performance results are highlighted with boldface. It is known from the table that our metric produces the best results, which produces the highest SRCC, KRCC, PLCC and lowest RMSE. S3 and SVC also produce better results than the rest of blind sharpness metrics.

To confirm the effectiveness of the proposed BQSVD, we compare our metric with the gray scale SVD method. Experimental results are shown in Table 2. We can observe that the proposed BQSVD model correlates highly with human visual perception of image sharpness, and it is remarkably superior to the gray scale SVD method. The SRCC value of the gray scale SVD method is 0.3066, while our metric is 0.4934. The performance improvement of the proposed method is larger than 37.9 % relative to the gray scale SVD method. Just as we discussed in Section 2.3, QSVD combines luminance and chrominance information into the IQA model and it can better describe the degree of the image distortion.

In the proposed method, the input color image is first converted to the LAB color space. In order to illustrate the necessity of the color space transformation, an experiment is conducted on the BID database. Pure quaternion is utilized to express image in RGB space and YIQ space [27] and the simulated results shown in Table 2. It can be observed from the table that LAB color space obtains best results. Just as analyzed before, the LAB color space includes all the visible colors for the human eye and is more suited to represent the color image.

Table 3 Performance comparison with eight popular general purpose blind methods on the BID database

Metric	PLCC	SRCC	KRCC	RMSE
BIQI [26]	0.4423	0.4024	0.2730	1.1228
DESIQUE [49]	0.2908	0.2924	0.1982	1.1978
NIQE [25]	0.4608	0.4584	0.3089	1.1111
BRISQUE [24]	0.2516	0.2138	0.1412	1.2117
DIIVINE [26]	0.3310	0.3427	0.2300	1.1814
BLLINDS-II [34]	0.0795	0.0870	0.0593	1.2480
CORNIA [4]	0.4611	0.4643	0.3110	1.1109
NFERM [11]	0.4738	0.4679	0.3183	1.1025
BQSVD (Pro.)	0.4988	0.4934	0.3379	1.0851

The best performed metric is highlighted with boldface

4.3 Comparison with general purpose blind IQA metrics

To verify the effectiveness of the proposed method, in this part, we compare our metric with the well-known general purpose blind IQA methods, including Distortion Identification-based Image Verity and INtegrity Evaluation (DIIVINE) [26], Codebook Representation for No-Reference Image Assessment (CORNIA) [4], NR Free Energy based Robust Metric (NFERM) [11], Blind Image Spatial QUality Evaluator (BRISQUE) [24], Blind Image Quality Index (BIQI) [26], BLind Image Integrity Notator using DCT Statistic (BLIINDS-II) [34], Natural Image Quality Evaluator (NIQE) [25], blind image quality assessment

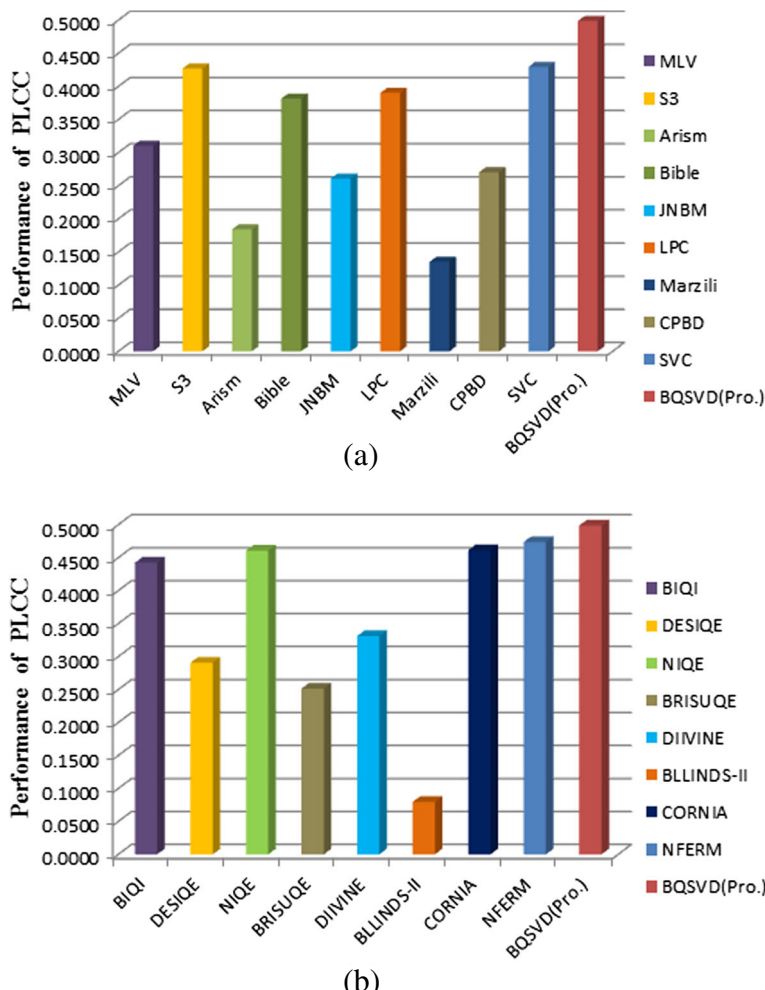


Fig. 9 Plots of the PLCC performance comparisons our blind BQSVD metric with popular IQA metrics on the BID database. **a** Comparison with bind sharpness metrics. **b** Comparison with blind general purpose IQA metrics

method based on Weibull statistics of log-derivatives of natural scenes (DESIQUE) [49]. Table 3 lists the experimental results, where the best results are highlighted with boldface.

It can be observed from the table that our metric produces the best results on the BID database. It further verifies the superiority of our method over the state-of-art general purpose blind IQA methods with respect to sharpness evaluation. NFERM [11] also creates promising results, and it outperforms the remaining blind general purpose blind quality assessment metrics.

Plots of the performance comparison are shown in Fig. 9. The vertical coordinate-axis Y represents the PLCC values of the compared algorithms. Figure 9a shows the PLCC values of the proposed method compare with the blind sharpness metrics, and Fig. 9b shows the PLCC values of the proposed method compare with blind general purpose IQA methods. It easily to find from the Fig. 9 that our metric get the highest accuracy of prediction.

We also conduct experiments on different kinds of real camera images deteriorated by different levels of blur distortion. Figure 10 shows four realistic blurred camera images with different subjective evaluate scores(MOS) and their sharpness scores obtained by the proposed method BQSVD. In Fig. 10, the strength of blur increase from (a) to (d), which also can be found from their MOS values. It can be seen from the figure that the proposed BQSVD method produces sharpness scores that decrease from (a) to (d), so the experiment results are highly consistent with human visual system.



Fig. 10 Four realistic blurred camera images and predicted objective scores by our proposed method BQSVD

5 Conclusions

In this paper, a blind quality index for camera images sharpness based on quaternion singular value decomposition is proposed. Comparison of our BQSVD with popular blind sharpness and general purpose blind measures are conducted on the BID database. Besides the substantially high prediction accuracy, it is worthy to emphasize three points below. First, experimental results demonstrate the superiority of the proposed metric on the BID database over state-of-art blind sharpness measures. Second, as far as we know, the proposed metric is the first to propose blind quality assessment based on hypercomplex singular value decomposition, which can well model realistic blurred images. Third, the proposed BQSVD metric only utilizes singular values to quantify the visual distortions. In the future work we will combine singular vectors together to evaluate the quality of camera images.

Acknowledgments This work is supported by National Natural Science Foundation of China under Grant 61379143, the Fundamental Research Funds for the Central Universities under Grant 2015QNA66, Science and Technology Planning Project of Nantong under Grant BK2014022 and the Qing Lan Project.

References

1. Attar A, Shahbahrami A, Rad RM (2016) Image quality assessment using edge based features. *Multimed Tools Appl* 75(12):1–16
2. Bahrami K, Kot AC (2014) A fast approach for no-reference image sharpness assessment based on maximum local variation. *IEEE Signal Process Lett* 21(6):751–755
3. Ciancio A, Da CA, Da SE, Said A, Samadani R, Obrador P (2011) No-reference blur assessment of digital pictures based on multifeature classifiers. *IEEE Trans Image Process* 20(1):64–75
4. Doeermann D, Kang L, Kumar J, Ye P (2012) Unsupervised feature learning framework for no-reference image quality assessment. In: Proc. IEEE Int Conf Computer Vision Pattern Recognition, vol 157, pp 1098–1105
5. Ferzli R, Karam LJ (2009) A no-reference objective image sharpness metric based on the notion of just noticeable blur (jnb). *IEEE Trans Image Process* 18(4):717–728
6. Gu K, Wang S, Yang H, Lin W, Zhai G, Yang X, Zhang W (2016) Saliency-guided quality assessment of screen content images. *IEEE Trans Multimed* 18(6):1098–1110
7. Gu K, Zhai G, Lin W, Liu M (2016) The analysis of image contrast: from quality assessment to automatic enhancement. *IEEE Trans Cybern* 46(1):284–297
8. Gu K, Zhai G, Lin W, Yang X, Zhang W (2015) No-reference image sharpness assessment in autoregressive parameter space. *IEEE Trans Image Process* 24(10):3218–31
9. Gu K, Zhai G, Lin W, Yang X, Zhang W (2015) Visual saliency detection with free energy theory. *IEEE Signal Process Lett* 22(10):1552–1555
10. Gu K, Zhai G, Yang X, Zhang W (2014) Hybrid no-reference quality metric for singly and multiply distorted images. *IEEE Trans Broadcast* 60(3):555–567
11. Gu K, Zhai G, Yang X, Zhang W (2015) Using free energy principle for blind image quality assessment. *IEEE Trans Multimed* 17(1):50–63
12. Gu K, Zhai G, Yang X, Zhang W, Chen CW (2015) Automatic contrast enhancement technology with saliency preservation. *IEEE Trans Circ Syst Vid Technol* 25(9):1480–1494
13. Hamilton WR (1844) Ii. on quaternions; or on a new system of imaginaries in algebra. The London Edinburgh, Dublin Philos Mag J Sci 25(163):10–13
14. Hassen R, Wang Z, Salama MMA (2013) Image sharpness assessment based on local phase coherence. *IEEE Trans Image Process* 22(7):2798–810
15. Huang Y, Chen X, Ding X (2016) A harmonic means pooling strategy for structural similarity index measurement in image quality assessment. *Multimed Tools Appl* 75(5):2769–2780
16. Kolaman A, Yadid-Pecht O (2012) Quaternion structural similarity: a new quality index for color images. *IEEE Trans Image Process* 21(4):1526–1536

17. Li J, Li X, Yang B, Sun X (2016) Segmentation-based image copy-move forgery detection scheme. *IEEE Trans Inf Forens Secur* 10(3):507–518
18. Li L, Cai H, Zhang Y, Lin W, Kot AC, Sun X (2016) Sparse representation-based image quality index with adaptive sub-dictionaries. *IEEE Trans Image Process* 25(8):3775–3786
19. Li L, Lin W, Wang X, Yang G, Bahrami K, Kot AC (2016) No-reference image blur assessment based on discrete orthogonal moments. *IEEE Trans Cybern* 46(1):39–50
20. Li L, Wu D, Wu J, Li H, Lin W, Kot AC (2016) Image sharpness assessment by sparse representation. *IEEE Trans Multimed* 18(6):1085–1097
21. Li L, Zhou Y, Lin W, Wu J, Zhang X, Chen B (2016) No-reference quality assessment of deblocked images. *Neurocomputing* 177:572–584
22. Liu H, Klomp N, Heynderickx I (2010) A no-reference metric for perceived ringing artifacts in images. *IEEE Trans Circ Syst Vid Technol* 20(4):529–539
23. Marziliano P, Dufaux F, Winkler S, Ebrahimi T (2004) Perceptual blur and ringing metrics: application to jpeg2000. *Signal Process Image Commun* 19(2):163–172
24. Mittal A, Moorthy AK, Bovik AC (2012) No-reference image quality assessment in the spatial domain. *IEEE Trans Image Process* 21(12):4695–708
25. Mittal A, Soundararajan R, Bovik AC (2013) Making a completely blind image quality analyzer. *IEEE Signal Process Lett* 20(3):209–212
26. Moorthy AK, Bovik AC (2010) A two-step framework for constructing blind image quality indices. *IEEE Signal Process Lett* 17(5):513–516
27. Narvekar ND, Karam LJ (2011) A no-reference image blur metric based on the cumulative probability of blur detection (cpbd). *IEEE Trans Image Process* 20(9):2678–2683
28. Narwaria M, Lin W (2012) Svd-based quality metric for image and video using machine learning. *IEEE Trans Syst Man Cybern Part B* 42(2):347–364
29. Narwaria M, Lin W, McLoughlin IV, Emmanuel S, Chia LT (2012) Fourier transform-based scalable image quality measure. *IEEE Trans Image Process* 21(8):3364–3377
30. Oh TH, Tai YW, Bazin JC, Kim H, Kweon IS (2016) Partial sum minimization of singular values in robust PCA: algorithm and applications. *IEEE Trans Pattern Anal Mach Intell* 38(4):744–758
31. Pan Z, Lei J, Zhang Y, Sun X (2016) Fast motion estimation based on content property for low-complexity h.265/hevc encoder. *IEEE Trans Broadcast* 1–10
32. Patent (2006) Image-quality estimation based on supercomplex singular-value decomposition, publ. nr.: CN1897634 A. <https://www.google.com/patents/CN1897634A?cl=en>
33. Qureshi MA, Deriche M, Beghdadi A (2016) Quantifying blur in colour images using higher order singular values. *Electrons Lett* 52(21):1755–1757
34. Saad MA, Bovik AC, Charrier C (2012) Blind image quality assessment: a natural scene statistics approach in the det domain. *IEEE Trans Image Process* 21(8):3339–3352
35. Sang QB, Wu XJ, Li CF, Lu Y (2014) Blind image blur assessment using singular value similarity and blur comparisons. *Plos One* 9(9):e108073–e108073
36. Sang Q, Qi H, Wu X, Li C, Bovik AC (2014) No-reference image blur index based on singular value curve. *J Vis Commun Image Represent* 25(7):1625–1630
37. Sangwine SJ, Le Bihan N (2006) Quaternion singular value decomposition based on bidiagonalization to a real or complex matrix using quaternion householder transformations. *Appl Math Comput* 182(1):727–738
38. Schanda J (2007) Colorimetry. Wiley-Interscience, p 61, ISBN 978-0-470-04904-4
39. Shnayderman A, Gusev A, Eskicioglu AM (2006) An svd-based grayscale image quality measure for local and global assessment. *IEEE Trans Image Process* 15(2):422–429
40. Soundararajan R, Bovik AC (2012) Rred indices: reduced reference entropic differencing for image quality assessment. *IEEE Trans Image Process* 21(2):517–526
41. Su B, Lu S, Tan C (2011) Blurred image region detection and classification. In: Proc. the 19th ACM international conference on multimedia, pp 1397–1400
42. Tang L, Li L, Gu K, Sun X, Zhang J (2016) Blind quality index for camera images with natural scene statistics and patch-based sharpness assessment. *J Vis Commun Image Represent* 40:335–344
43. Torkamani-Azar F, Amirshahi SA (2007) A new approach for image quality assessment using SVD. In: Proc. IEEE int. symp. signal processing and its applications, pp 1–4
44. VQEG (2000) Final report from the video quality experts group on the validation of objective models of video quality assessment, <http://www.vqeg.org/>
45. Vu PV, Chandler DM (2012) A fast wavelet-based algorithm for global and local image sharpness estimation. *IEEE Signal Process Lett* 19(7):423–426

46. Vu CT, Phan TD, Chandler DM (2012) S3: a spectral and spatial measure of local perceived sharpness in natural images. *IEEE Trans Image Process* 21(3):934–945
47. Xia Z, Wang X, Zhang L, Qin Z, Sun X, Ren K (2016) A privacy-preserving and copy-deterrence content-based image retrieval scheme in cloud computing. *IEEE Trans Inf Forens Secur* 11(11):2594–2608
48. Yong W, Yuqing W, Xiaohui Z (2016) Complex number-based image quality assessment using singular value decomposition. *IET Image Process* 10(2):113–120
49. Zhang Y, Chandler DM (2013) No-reference image quality assessment based on log-derivative statistics of natural scenes. *J Electron Imag*
50. Zhang L, Zhang L, Bovik AC (2015) A feature-enriched completely blind image quality evaluator. *IEEE Trans Image Process* 24(8):2579–91
51. Zhou Z, Wang Y, Wu QM, Yang C, Sun X (2017) Effective and efficient global context verification for image copy detection. *IEEE Trans Inf Forens Secur* 12(1):48–63



Lijuan Tang received the B.E. degree from Jiangsu Normal University, China, in 2005, and the master's degree with the University of Mining and Technology, China, in 2008. She is currently working toward the Ph.D degree in information and electrical engineering at the China University of Mining and Technology, Xuzhou, China. Her research interests include image quality assessment and visual perceptual modeling.



Qiaohong Li received the B.E. and M.E. degree in School of Information and Communication Engineering from Beijing University of Posts and Telecommunications, Beijing, China. She is now currently pursuing the Ph.D degree with the school of Computer Engineering, Nan Yang Technological University, Singapore. Her research interests includ image quality assessment, speech quality assessment, computer vision, and visual perceptual modelling.



Leida Li received the B.S. and Ph.D. degrees from Xidian University, Xi'an, China, in 2004 and 2009, respectively. From January 2014 to January 2015, he was a Visiting Research Fellow in the School of Electrical and Electronic Engineering, Nanyang Technological University, Singapore. Currently, he is a professor in the School of Information and Electrical Engineering, Author Biographies Click here to download Author Biographies Mul_Biography.pdf China University of Mining and Technology, China. His research interests include multimedia quality assessment, information hiding and image forensics.



Ke Gu received the B.S. and PhD degrees in electronic engineering from Shanghai Jiao Tong University, Shanghai, China, in 2009 and 2015. He is the reviewer for IEEE T-IP, T-CSVT, T-MM, T-CYB, TBC, SPL, Neurocomputing, SPIC, JVCI, SIViP, Information Sciences, etc. He has reviewed more than 30 journal papers each year. His research interests include quality assessment, contrast enhancement and visual saliency detection. Dr. Gu received the Best Paper Award at the IEEE International Conference on Multimedia and Expo (ICME) 2016.



Jiansheng Qian received the B.E. degree from Xidian University, Xi'an, China, in 1985, and the master's degree from Xi'an Institute of Optics and Precision Mechanics, Chinese Academy of Sciences, Xi'an, China, in 1988, and the Ph.D degree in 2003. He is currently a Professor of China University of Mining and Technology, China. His research interests include the areas of signal processing for communication, broadband network technology and application, coal mine communication and monitoring.